Electron-Transfer Dynamics in DTDCI/MoS_2 and DTDCI/WS_2 Nanoclusters

C. I. Butoi, B. T. Langdon, and D. F. Kelley*

Department of Chemistry, Colorado State University, Fort Collins, Colorado 80523-1872

Received: July 14, 1998; In Final Form: September 9, 1998

The kinetics of forward and reverse electron transfer (ET) between an organic cyanine dye and semiconductor nanoclusters have been studied. The systems studied are MoS_2/DTDCI and WS_2/DTDCI (DTDCI ≡ diethylthiodicarbocyanine iodide). The static spectroscopy of these systems indicates that the dye adsorbs on the nanoclusters as monomers. The vast majority of excited-state dye molecules are quenched by rapid (<10 ps) electron injection in the nanocluster. The reverse ET kinetics are elucidated by time-resolved absorption (bleach recovery) measurements. The results indicate that there are two components of reverse ET that take place on the tens to hundreds of picoseconds and >10 ns time scales. These components are assigned to reverse ET from shallow (tens to hundreds of picoseconds) and deep (>10 ns) trap states. The shorter time scale component is nonexponential and is fit with distributed kinetics model, in which the Bohr radius of the trapped electron is about 2.2 nm. This value of the Bohr radius is comparable to that obtained from electron/hole recombination studies.

Introduction

Electron transfer (ET) at semiconductor interfaces is involved in many processes that are of great practical as well as fundamental importance. These include photography, solar energy conversion, and photocatalysis.[1,2] Interfacial ET may result in charge separation, which drives these processes. Dyes can be adsorbed on semiconductors and, following photoexcitation, may inject electrons into the semiconductor.[3] Charge separation may then occur in competition with reverse ET, which restores the oxidized dye molecule to its original state. The dynamics of both the forward and reverse ET processes are of crucial importance in determining the efficiency of charge separation.

Electron transfer from excited-state dyes into nanocrystalline semiconductors (specifically TiO_2) and semiconductors particles has recently received a great deal of attention.[1,2,4−18] Most studies have found that this process occurs very quickly—typically in less than a picosecond—although in some cases, slower rates are observed.[18] Rapid ET is explained in terms of the large density of acceptor states in the semiconductor conduction band.[2,19] Although of equal importance in determining the efficiency of charge separation, far less attention has been given to the dynamics of reverse ET. In most cases, reverse ET is very much slower than forward ET (dye to nanocluster electron injection).[4−6] There are two major reasons why this is expected to be the case. First, forward ET takes place into a dense manifold of accepting conduction band states. In contrast, reverse electron transfer is to a single oxidized dye state. Second, reverse ET is often highly exothermic, and the resulting Franck−Condon factors for this process are quite small; i.e., reverse ET is typically far into the Marcus inverted region. Reverse ET times are usually on the order of 100 times slower than forward times and usually occur on the 10−100 ps time scale. This time scale is comparable to that observed for interfacial ET involving adsorbed electron acceptors.[20,21] In these studies a semiconductor nanocluster is photoexcited, creating an electron/hole pair. Electron/hole recombination then competes with electron transfer to adsorbed electron acceptors. In this case, the ET rate varies with the energetic driving force, but when the driving force is larger than a few tenths of an electronvolt, a tens to hundreds of picoseconds ET time scale is observed.[20,21]

Although the rates of reverse ET have been measured for several types of dye/semiconductor systems, very little is known about the dynamics of this process. Specifically, the roles of ET from the conduction band and from localized surface trap states have not been studied. Three distinct ET mechanisms can be imagined. ET could occur from the conduction band (with no involvement of trap states), from the conduction band being thermally populated from trap states, or directly from trap states. Very different kinetics are expected in these three cases. Direct ET from the conduction band would lead to single-exponential kinetics. Thermal population of the conduction band would also result in exponential kinetics if all the traps were the same depth. Any variation in trap depths would, however, lead to a distribution of Boltzmann factors and therefore nonexponential kinetics. These kinetics would be expected to be very complicated and, without knowing the distribution of trap depths, very difficult to model. Electron transfer directly from trap states is expected to yield ET rates that vary with the separation between the electron trap and the oxidized dye, thus giving rise to nonexponential kinetics. In this case, the extent to which the kinetics are nonexponential depends on the spatial extent of the trapped electron and the size of the nanocluster. With an assumed nanocluster geometry, these kinetics are very straightforward to model, as discussed below.

There are two other situations in which electron transfer is quite analogous to the reverse ET process reported here. Electron/hole recombination and electron transfer to adsorbed acceptors can both occur following band gap photoexcitation and thus production of an electron/hole pair within the nanocluster. These processes are similar to reverse ET in the sense that in all cases an electron is transferred to an acceptor (the

* To whom correspondence should be addressed.

10.1021/jp983008s CCC: $15.00
Published on Web 11/05/1998

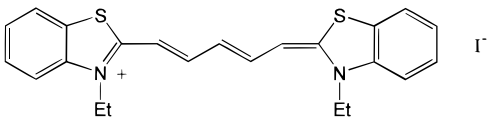

Figure 1. Structure of the DTDCI molecule.

oxidized dye, an acceptor molecule, or the trapped hole) at the nanocluster edge. We have recently shown that ET occurs directly from trap states in these situations.[20,21,23] Specifically, we have applied a distributed kinetics model based on ET directly from trap states to interpret the nonexponential kinetics observed in the recombination of the trapped electrons and holes,[21] and a similar distributed kinetics model has also been successfully applied to ET from excited MoS_2 nanoclusters to adsorbed electron acceptors.[23]

In this paper, we examine the kinetics of forward and reverse ET involving DTDCI adsorbed on MoS_2 and WS_2 nanoclusters. DTDCI is a cyanine dye (see Figure 1) that absorbs strongly in the red region of the visible spectrum. The dye has a relatively long-lived excited state (nanoseconds), which is easily oxidized. Like other cyanine dyes, DTDCI will inject an electron into many different types of semiconductors.[3] We show that DTDCI adsorbs as monomers on MoS_2 or WS_2 nanoclusters and rapidly injects an electron into the semiconductor conduction band. We examine the kinetics of reverse ET and show that these kinetics from shallow traps are nonexponential and may be described by a distributed kinetics model.

Experimental Section

MoS_2 and WS_2 nanoclusters are synthesized in inverse micelles using procedures that have been previously described.[24,25] These nanoclusters are synthesized in tridodecylmethylammonium iodide (TDAI)/hexanol/octane tertiary micelles or, in some cases, the analogous chloride micelles. Following synthesis, the nanoclusters are extracted into an equal volume of acetonitrile. MoS_2 is a layered material, consisting of sheets of S−Mo−S covalently bound trilayers, with the each of the trilayers separated by a large van der Waals gap.[26] Preliminary STM studies, along with the analogy to the structurally similar PtS_2 nanoclusters,[27] suggest that these nanoclusters consist of single S−Mo−S trilayer disks. These nanoclusters exhibit an absorption maximum at about 370 nm, and previous studies have shown that MoS_2 nanoclusters with a 370 nm absorption maximum have diameters of about 3.0 nm.[23,24] Assuming a single trilayer morphology, the 3.0 nm diameter nanoclusters contain about 70 Mo atoms. Typical concentrations are $[Mo] = 1 \times 10^{-3}$ M, and we conclude that the nanocluster concentrations are about 1.4×10^{-5} M. WS_2 nanoclusters are synthesized in exactly the same way as the MoS_2 nanoclusters. While the WS_2 nanoclusters have not been as well characterized as their Mo analogues, the two types of nanoclusters appear to be similar in terms of nanocluster size, spectroscopy, and surface chemistry.

The nanoclusters may be manipulated into a variety of different solvents. Following synthesis in inverse micelles, the nanoclusters may be extracted into acetonitrile, indicating that the nanoclusters are initially charged. These nanoclusters may then be neutralized and put into nonpolar solutions in either of two ways. First, the acetonitrile nanocluster solution may be evaporated to dryness and the nanoclusters resuspended in toluene. The entire nanocluster sample dissolves in toluene, leaving no residue of aggregated nanoclusters. The solubility in toluene indicates that their charge has been removed in this process. Alternatively, following extraction into acetonitrile, a small amount of water may be added and the nanoclusters reextracted into a clean octane phase. Both of the above procedures have no observable effect on the nanocluster absorption spectrum, indicating that these procedures cause little or no aggregation.

Variations of the above nanocluster manipulations may be used to adsorb DTDCI onto the nanoclusters by either of two methods. First, a film of DTDCI on a glass surface is prepared by evaporation of a dye solution. A toluene solution of nanoclusters (produced by evaporation from acetonitrile followed by resuspension in toluene) is then put in contact with the dye film. Some portion of the dye goes into the nanocluster/toluene solution. DTDCI is a cationic dye and is totally insoluble in nonpolar solvents such as toluene or octane. The presence of the dye in the toluene solution therefore indicates that the dye is attached to the toluene-soluble nanoclusters.

Alternatively, following extraction into acetonitrile reextraction into octane, a small volume of a concentrated dye solution in acetonitrile is added to the nanocluster octane solution. The solution separates into acetonitrile and octane phases, with most of the dye going into the octane phase. In the absence of the nanoclusters, the dye remains entirely in the acetonitrile phase, indicating that this procedure also results in dye adsorption to the nanoclusters. Both procedures result in the nanoclusters being saturated with DTDCI. In both cases, the net dye concentrations are about 2×10^{-5} M, corresponding to an average of about 1.4 dye molecules per nanocluster.

Time-resolved absorbance measurements were made using a picosecond absorption spectrometer, which has been previously described.[28] The excitation and probe wavelengths were 532 and 660 nm, respectively. The 532 and 660 nm pulses have temporal widths of about 35 and 10 ps, respectively, and the resulting temporal resolution is slightly over 35 ps. Pulse intensities were kept sufficiently low that at most about 10% of the dyes are excited. Thus, the probability of having two or more excited dyes on any one nanocluster is negligibly small.

Emission kinetics were obtained using a time-correlated single-photon-counting apparatus, which has been previously described.[29] This case also corresponds to the low-intensity limit, with there being a negligibly small probability of having two or more excited dyes on any one nanocluster.

Results and Discussion

Static Spectroscopy. The static absorption spectrum of DTDCI in acetonitrile is shown in Figure 2. The absorbance maximum is at 653 nm, in agreement with previous results.[3] It is not possible to obtain an absorption spectrum of DTDCI in toluene or octane, since DTDCI is insoluble in these solvents. The static absorption spectrum of the MoS_2 nanoclusters with adsorbed DTDCI in toluene is also shown in Figure 2. Two sets of absorption features are observed. The strong peak at 370 nm along with features to the blue of this peak are identical to those previously reported for 2.5−3.0 nm diameter MoS_2 nanoclusters.[24,25] The lack of any change in these features indicates that the dye does not cause nanocluster aggregation or dissolution and does not significantly perturb the nanocluster electronic structure. The features in the 550−700 nm region are quite similar to those observed for the free dye and are assigned to DTDCI adsorbed on the MoS_2 nanoclusters. The wavelength maximum of this peak remains constant at 673 nm when the nanocluster concentration is held constant and the dye is diluted by a factor of 2000. We also note that the spectral shift (∼20 nm) compared to solution-phase dye monomers is relatively small and is considerably less than is typically

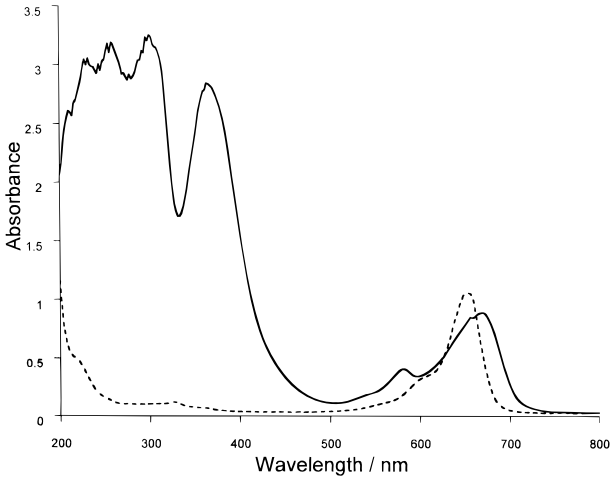

Figure 2. Static absorption spectra of DTDCI in acetonitrile (dotted curve) and of MoS_2 nanoclusters in toluene with adsorbed DTDCI dye (solid curve).

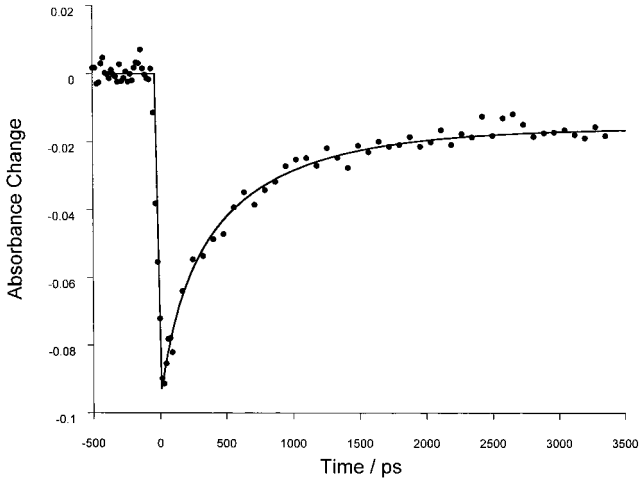

Figure 3. Transient absorption (bleach recovery) kinetics of MoS_2/DTDCI nanoclusters in toluene. The pump and probe wavelengths are 532 and 680 nm, respectively. Also shown is a curve calculated on the basis of the distributed kinetics model discussed in the text and convoluted with the instrument response function.

observed for J-aggregates (50−100 nm).[30] These observations suggest that there are dye monomers, rather than aggregates, adsorbed on the nanoclusters. The intensity of this absorption is also consistent with this assignment. Based on the solution-phase extinction coefficient of 2.5×10^5, the adsorbed dye concentration is about 2×10^{-5} M. Thus, with a nanocluster concentration of 1.4×10^{-5} M, there is an average of 1.4 adsorbed dyes per nanocluster. The 30 Å diameter nanoclusters have a circumference of about 100 Å. DTDCI molecules have an end-to-end distance of approximately 22 Å. The dyes would be expected to attach to the nanoclusters by interaction of the sulfurs with the Mo atoms at the nanocluster edge, resulting in the dye being stretched out along the nanocluster edge. In this geometry, there can be a maximum of about 4 dye molecules per nanocluster. The above average value of 1.4 dyes per nanocluster is thus consistent with this limit.

Electron Injection. Excitation of the dye/nanocluster hybrids at 532 or 670 nm results in very weak emission—1−2 orders of magnitude weaker than is obtained from a comparable concentration of the free dye in acetonitrile solution. This quenching could be due to electron injection into the nanocluster or due to rapid radiationless decay resulting from adsorption onto the nanocluster. The latter possibility seems quite unlikely, since adsorption to the nanocluster causes no dye aggregation and only a small perturbation of the dye absorption spectrum. Thus, the quenching is due to rapid electron transfer from the excited-state dye into the nanocluster conduction band. Time-resolved studies indicate that the observed emission exhibits a single-exponential decay with an approximately 2 ns time constant. This decay time is comparable to the decay time of the free dye in acetonitrile. We conclude that a small fraction (a few percent) of the adsorbed dyes do not inject electrons into the nanoclusters and simply emit on the same time scale as free dye molecules in solution. It is important to note that no fast decay component is observed in the emission kinetics. If electron injection was occurring on the time-correlated photon-counting time scale (50 ps), or even an order of magnitude faster than this, then a pulse width limited emission decay component would be observed. The lack of any observed fast decay indicates that electron injection must be faster than a few picoseconds. This conclusion is consistent with other studies of excited-state dyes injecting electrons into semiconductors. In most cases, the electron-transfer process occurs on the subpicosecond time scale.

Reverse Electron Transfer. Time-resolved absorption (bleach recovery) kinetics for MoS_2/DTDCI in toluene are shown in Figure 3. The pump and probe wavelengths are 532 and 660 nm, respectively. The nanoclusters have essentially no absorption at 532 nm, and the pump pulse only excites the adsorbed dye. The excited-state dye rapidly injects an electron into the nanocluster, and the negative absorbance change indicates a loss of ground-state dye population. Reverse ET is the rate-limiting process in ground-state repopulation, and the observed kinetics are thus indicative of the rate of reverse ET. These kinetics exhibit two distinct components: a nonexponential decay that occurs on the time scale of a few hundred picoseconds and a much slower (>10 ns) decay, which appears as an approximately constant component on the time scale of Figure 3. Both components are due to repopulation of the dye ground state and thus reflect fast and slow reverse electron transfer rates. The fraction of the kinetic decay that corresponds to the slow (constant) component varies from sample to sample but is generally 15−50% of the total. The presence of the slow reverse ET component has two possible explanations. First, this fraction (15−50%) of the dyes may be much more weakly coupled to the nanoclusters, or second, this fraction of the nanoclusters has very deep electron traps, from which ET occurs quite slowly. While either situation could result in the slow reverse ET component, the first possibility is unlikely for two reasons. Very weak dye/nanocluster electronic coupling would be expected to also result in slow electron injection, and this is not observed (except for a very small fraction of dyes that do not inject at all). The static spectroscopy also argues against the first explanation. Figure 2 shows that the adsorbed dyes have an absorption maximum that is about 20 nm red of the free dye absorption maximum. Weakly coupled dyes would be expected to have a smaller spectral shift than the strongly coupled dyes, and the observed 20 nm shift would represent a weighted average of the two types of dyes. The relative magnitudes of the fast (few hundred picoseconds) and slow (>10 ns) components would reflect the fraction of weakly coupled dyes in that sample. If the bleach recovery time scale is correlated to the magnitude of the spectral shift, then there should be differences in static spectra comparing samples with large and small amounts of the slow component. However, comparison of the static spectra of these samples reveals no significant differences in the shape of the peak or the absorption

maximum. We conclude that the most likely situation is that there are two distinct types of electron traps, giving rise to the different kinetic components. Deep traps are expected to be more localized than shallow traps, and the overlap with the oxidized dye (the electron acceptor) is less in the deep trap case. The reduced overlap would be expected to result in slower reverse ET. The slow component is the smaller of the two components. In what follows, we will analyze only the faster component, which is associated with the shallower traps.

Reverse ET is quite analogous to electron/hole recombination, since in the electron/hole recombination case the electron is also being transferred to an acceptor (a trapped hole) at the nanocluster edge. We have recently studied the dynamics of electron/hole recombination and shown that the electron/hole recombination kinetics may be described by a distributed kinetics model.[21] The main assumptions of the model are the following. (1) Relaxation of trapped electrons and holes is fast compared to recombination, and the positions of electrons and holes are fixed as recombination occurs. (2) Prior to any recombination, trapped electrons and holes are distributed randomly on the edges of the disklike (assumed circular) nanocluster. (3) The recombination rates are given by the product of a separation-independent term (the square of a matrix element) and an exponential dependence of the electron/hole separation. The above approximations result in a time-dependent distribution of electron/hole separations which is given by

$$P(r,t) = (1 - (r/d)^2)^{-1/2} \exp(-(k_r(r) + k_{nr}(r))t) \qquad (1)$$

where r is the electron/hole separation, d is the nanocluster diameter, and $k_r(r)$ and $k_{nr}(r)$ are the separation-dependent radiative and nonradiative recombination rate constants, respectively. Because of its smaller effective mass, the electron is far more delocalized than the hole, and the distance dependence of these rates is determined by the electron Bohr radius. Specifically,

$$k_{nr}(r) = |V|^2 \exp(-2r/a_0) \quad \text{and} \quad k_r(r) = |\mu|^2 \exp(-2r/a_0) \qquad (2)$$

where V and μ are the Franck−Condon weighted matrix elements for nonradiative and radiative decays, respectively, and a_0 is the trapped electron Bohr radius. The time-dependent emission intensity is given by

$$I(t) = \int_0^d k_r(r)\, P(r,t)\, dr \qquad (3)$$

The above model has two adjustable parameters: a_0 and the quantity $(|V|^2 + |\mu|^2)$. Typically, a_0 values in the range 2.0−2.5 nm are obtained from the emission decay curves. These a_0 values may be understood in terms of the electron effective mass and dielectric constant. Bulk MoS_2 has an electron effective mass of about $0.18m_e$ and a dielectric constant of about 6.8. These values yield a calculated Bohr radius of 2.0 nm, which also corresponds to the known exciton Bohr radius.[31] We note that this model describes the MoS_2 nanocluster emission kinetics quite well, while assuming that all the electron traps are of the same depth. Thus, these studies of electron/hole recombination do not indicate the presence of the deep electron traps postulated above. However, emission studies are quite insensitive to the presence of deep electron traps. This is because the emission intensity depends on k_r, as given by eq 3. Since the deeply trapped electrons are highly localized (small values of a_0), the values of $k_r(r)$ associated with these electrons drop off rapidly with r and, as a result, are generally quite small (see eq 2).

This same basic distributed kinetics model may be applied in the present dye/reverse electron-transfer case. However, the transient absorption experiment simply examines the ground-state dye population. In this case, the signal intensity does not depend on the radiative lifetime. Specifically,

$$\Delta A/A = -\int_0^d P(r,t)\, dr \qquad (4)$$

where $P(r,t)$ is given by eq 1 and $k_r = 0$. The nonradiative rate is simply the (distance-dependent) reverse ET rate, $k_{nr}(r) = k'_{et} \exp(-2r/a_0)$. As a result, whereas the deep electron traps are not detected in the electron/hole recombination studies, the entire trapped electron population is detected here, with the deeply trapped electrons giving rise to the slow component. Figure 3 also shows a curve calculated on the basis of eq 4, considering only the shallow trapped electrons. The slow reverse ET kinetics are taken to be a constant component on this time scale, with the amount of this constant component (i.e., the fraction of nanoclusters with deep electron traps) simply taken as an adjustable parameter. The calculated curve in Figure 3 corresponds to a 17% constant component and k_{et} and a_0 values of $(70\ ps)^{-1}$ and 2.2 nm, respectively. We note that while the fraction of slow component varies from sample to sample, the a_0 values are constant within the experimental error (about ±15%). This value of a_0 is within experimental error of that obtained from electron/hole recombination studies. This is not at all surprising because the two different sets of kinetics pertain to the same population of electron traps. It should be noted that integration of eq 4 gives nonexponential kinetics because of the separation dependence of $k_{nr}(r)$ in eq 2; i.e., this is an inherent feature of the model.

It is of interest to compare these results to those obtained where the electron acceptor is an adsorbed 2,2′-bipyridine. In this case, band gap excitation produces an electron/hole pair that may undergo trapping and then radiative or nonradiative recombination. The trap emission from trapped electrons and holes may be quenched by electron transfer to the adsorbed bipyridine.[23] The emission kinetics have been analyzed using a distributed kinetics model similar to that described above, and the results yield a considerably smaller value of a_0, 0.7 nm. This difference may be understood in terms of differences in binding of the bipyridine and oxidized dye as electron acceptors. The dye is very strongly attached and is thus very strongly electronically coupled to the nanocluster. All of the electronic coupling is through the nanocluster, just like in the electron/hole recombination case. In contrast, the bipyridine electron acceptors are not as strongly attached, and some of the electronic coupling occurs through the surrounding solvent. The Bohr radius of the trapped electron depends on the (high-frequency) dielectric constant and the electron effective mass. When electron transfer occurs by coupling through the solvent, the appropriate dielectric constant is the high-frequency dielectric constant of the solvent,[32] and the appropriate mass is simply the electron mass. For acetonitrile, this results in a calculated a_0 value of 0.095 nm, which is much smaller than the 2.0 nm value appropriate to MoS_2. Thus, to the extent that electron transfer occurs by coupling through the solvent in the bipyridine case, it is a more distance-dependent and a shorter-range process than if it occurs by coupling through the nanocluster.

Analogous studies have been performed on WS_2 nanoclusters with adsorbed DTDCI dye. The results are in every way indistinguishable from those presented above for MoS_2. This

result is actually not too surprising; molybdenum and tungsten as well as their disulfides have very similar chemical properties. MoS_2 and WS_2 have the same bulk crystal structure and almost surely have the same structures as nanoclusters. The lattice constants of bulk MoS_2 and WS_2 are almost identical,[33] as are their direct and indirect band gaps.[34] Reaction of the metal tetrachloride with H_2S in inverse micelles results in very similar absorption spectra, indicating comparably sized nanoclusters in both cases. In light of the similarity of the bulk properties and the nanocluster formation chemistry, it is not surprising that the nanocluster edge traps of the two materials are quite similar.

Conclusions

Several conclusions may be drawn from the results presented here.

1. Cyanine dyes are readily adsorbed onto MoS_2 and WS_2 nanoclusters. The static spectroscopy indicates that there are an average of 1.4 dyes per nanocluster and that the dyes are adsorbed as monomers.

2. Following photoexcitation, the excited-state dye rapidly (less than a few picoseconds) injects an electron into the nanocluster conduction band.

3. The conduction band electron is rapidly localized into shallow or deep electron traps at the nanocluster edges. Most nanoclusters have only shallow traps.

4. Reverse electron transfer occurs slowly from the deep traps ($<$10 ns) and comparatively rapidly from the shallow traps. The latter process may be described by a distributed kinetics model, similar to the one used to describe electron/hole recombination.

Acknowledgment. This work was supported by a grant from the Department of Energy (Grant DE-FG03-96ER14717).

References and Notes

(1) For a recent and comprehensive review see: *Semiconductor Nanoclusters−Physical, Chemical and Catalytic Aspects*; Kamat, P. V., Meisel, D., Eds.; Elsevier: Amsterdam, 1997.

(2) Miller, R. J. D.; McLendon, G. L.; Nozik, A. J.; Schmickler, W.; Willig, F. In *Suface Electron-Transfer Processes;* VCH: New York, 1995; Chapter 5.

(3) Parkinson, B. A. *Langmuir* **1988**, *4*, 967.

(4) Martini, I.; Hartland, G. V.; Kamat, P. V. *J. Phys. Chem. B* **1997**, *101*, 4826.

(5) Martini, I.; Hodak, J.; Hartland, G. V.; Kamat, P. V. *J. Chem. Phys.* **1997**, *107*, 8064.

(6) Kamat, P. V.; Das, S.; Thomas, K. G.; George, M. V. *Chem. Phys. Lett.* **1991**, *178*, 75.

(7) Murakoshi, K.; Yanagida, S.; Capel, M.; Castner, E. W. Presented at the ACS Symposium, Nanostructured Materials: Clusters, Composites and Thin Films, April 13−17, 1997.

(8) Bechinger, C.; Ferrere, S.; Zaban, A.; Sprauge, J.; Gregg, B. A. *Nature* **1996**, *383*, 608. Zaban, A.; Ferrrere, S.; Gregg, B. A. *J. Phys. Chem. B* **1998**, *102*, 452.

(9) Lindstrom, H.; Rensmo, H.; Sodengren, S.; Solbrand, A.; Lindquist, S. E. *J. Phys. Chem.* **1996**, *100*, 3084.

(10) Cao, F.; Oskam, G.; Meyer, G. J.; Searson, P. C. *J. Phys. Chem.* **1996**, *100*, 17021.

(11) Konenkamp, R.; Wahi, A.; Hoyer, P. *Thin Solid Films* **1996**, *246*, 13. Boschloo, G. K.; Goossens, A.; Schoonman, J. *J. Electroanal. Chem.* **1997**, *428*, 25.

(12) Heimer, T. A.; Heilweil, E. J. *J. Phys. Chem. B* **1997**, *101*, 10990.

(13) Fessenden, R. W.; Kamat, P. V. *J. Chem. Phys.* **1995**, *99*, 12902. Lui, D.; Kamat, P. V. *J. Chem. Phys.* **1996**, *105*, 965. Kamat, P. V. *J. Phys. Chem.* **1989**, *93*, 859. Kamat, P. V.; Chauvet, J.-P.; Fessenden, R. W. *J. Phys. Chem.* **1986**, *90*, 1389.

(14) Hagfeldt, A.; Gratzel, M. *Chem. Rev.* **1995**, *95*, 49. Rehm, J. M.; McLendon, G. L.; Nagasawa, Y.; Yoshihara, K.; Moser, J.; Gratzel, M. *J. Phys. Chem.* **1996**, *100*, 9577. Tachibana, Y.; Moser, J. E.; Gratzel, M.; Klug, D. R.; Durrant, J. R. *J. Phys. Chem* **1996**, *100*, 20056.

(15) Burfeindt, B.; Hannappel, T.; Storck, W.; Willig, F. *J. Phys. Chem.* **1996**, *100*, 16463.

(16) Rabani, J.; Ushida, K.; Koichi, Y.; Stark, J.; Gershuni, S.; Kira, A. *J. Phys. Chem. B* **1997**, *101*, 3136.

(17) Argazzi, R.; Bignozzi, C. A.; Heimer, T. A.; Castellano, F. N.; Meyer, G. J. *Inorg. Chem.* **1994**, *33*, 5471. Argazzi, R.; Bignozzi, C. A.; Heimer, T. A.; Meyer, G. J. *Inorg. Chem.* **1996**, *36*, 2. Heimer, T. A.; D'Arcangelis, S. T.; Farzad, F.; Stipkal, J. M.; Meyer, G. J. *Inorg. Chem.* **1996**, *35*, 5319.

(18) Liu, D.; Kamat, P. V.; George, K.; Thomas, J. K.; Das, S.; George, M. V. *J. Chem. Phys.* **1996**, *106*, 6404.

(19) Lanzafame, J. M.; Palese, S.; Wang, D.; Miller, R. J. D.; Muenter, A. A. *J. Phys. Chem.* **1994**, *98*, 11020.

(20) Parsapour, F.; Kelley, D. F.; Craft, S.; Wilcoxon, J. P. *J. Chem. Phys.* **1996**, *104*, 4978.

(21) Doolen, R.; Latinen, R.; Parsapour, F.; Kelley, D. F. *J. Phys. Chem. B* **1998**, *102*, 3906.

(22) Rossetti, R.; Brus, L. E. *J. Phys. Chem.* **1986**, *90*, 558.

(23) Parsapour, F.; Kelley, D. F.; Wilcoxon, J. P., to be published.

(24) Wilcoxon, J. P.; Williamson, R. L.; Baughman, R. *J. Chem. Phys.* **1993**, *98*, 9933. (b) Wilcoxon, J. P.; Baughman, R. J.; Williamson, R. L. In *Novel Methods for Catlayst Preparation*; Symposium S, Proceedings of the Fall Meeting of the Materials Research Society, Boston, MA, Nov 1990.

(25) Wilcoxon, J. P.; Samara, G. A. *Phys. Rev. B* **1995**, *51*, 7299.

(26) Gerischer, H. In *Topics in Applied Physics*; Seraphin, B. O., Ed.; Springer: Berlin, 1979; Vol. 31.

(27) Parsapour, F.; Kelley, D. F.; Williams, R. S. *J. Phys. Chem. B*, submitted.

(28) Larson, S. L.; Elliott, C. M.; Kelley, D. F. *Inorg. Chem.* **1996**, *35*, 2070.

(29) Nimlos, M. R.; Young, M. A.; Bernstein, E. R.; Kelley, D. F. *J. Chem. Phys.* **1989**, *91*, 5268.

(30) Khairutdinov, R. F.; Serpone, N. *J. Phys. Chem. B* **1997**, *101*, 2602.

(31) Coehoorn, R.; Haas, C.; Dijkstra, J.; Flipse, C. J. F.; deGroot, R. A.; Wold, A. *Phys. Rev. B* **1987**, *35*, 6195, 6203. (b) Evans, B. L.; Young, P. A *Proc. R. Soc. London, A* **1965**, *284*, 402.

(32) Bordewijk, P. *Theory of Electric Polarization*; Elsevier: Amsterdam, 1978; Vol. II.

(33) Levy, F. *Crystallography and Crystal Chemistry of Materials with Layered Structures*; Reidel: Holland, 1976; p 2.

(34) Kam, K. K.; Parkinson, B. A. *J. Phys. Chem.* **1982**, *86*, 463.